Giga- and terahertz frequency band detector based on an asymmetrically necked n-n+-GaAs planar structure

A. Suziedelis, J. Gradauskas, S. Asmontas, G. Valusis, and H. G. Roskos

Citation: J. Appl. Phys. **93**, 3034 (2003); doi: 10.1063/1.1536024
View online: http://dx.doi.org/10.1063/1.1536024
View Table of Contents: http://jap.aip.org/resource/1/JAPIAU/v93/i5
Published by the American Institute of Physics.

Giga- and terahertz frequency band detector based on an asymmetrically necked n-n^+-GaAs planar structure

A. Sužiedelis, J. Gradauskas, and S. Ašmontas
Semiconductor Physics Institute, A. Goštauto 11, LT-2600, Vilnius, Lithuania

G. Valušis[a] and H. G. Roskos
Physikalisches Institut, J. W. Goethe Universität, Robert-Mayer Str. 2-4 D-60054 Frankfurt/M, Germany

(Received 6 November 2002; accepted 13 November 2002)

We describe the concept of an asymmetrically shaped n-n^+-planar GaAs diode whose operation is based on nonuniform free charge carrier heating effects. The detector was fabricated on thin elastic polyimide film and has been shown to have an operational bandwidth for detection ranging from 30 GHz up to 2.5 THz at room temperature. The voltage sensitivity of the detector is nearly independent of the frequency from 30 GHz up to 0.7 THz and is close to 0.3 V/W. In the upper section of the frequency range, 0.7–2.5 THz, the sensitivity is limited by the electron momentum relaxation time. The induced signal responds linearly to the incident power over the frequency range studied. It is shown that the performance of the detector can be explained well by a phenomenological theory. © *2003 American Institute of Physics.* [DOI: 10.1063/1.1536024]

I. INTRODUCTION

Development of compact and reliable detectors operating within a broad frequency band of electromagnetic radiation is an important issue in the rapidly evolving terahertz (THz) and subterahertz electronics. Depending on an absolute frequency scale, the physical principles behind detector operation can be completely different. For instance, microwave detectors at gigahertz (GHz) frequencies such as point-contact whisker-type diodes or sensors based on a change of semiconductor electrical resistance at high electric fields[1,2] usually employ classical carrier transport in bulk or specifically formed regions of a semiconductor. The cutoff frequency of these detectors lies, as a rule, below several hundreds of GHz. For the detection of infrared radiation, intersubband transitions in semiconductor nanostructures seem to be the most promising choice. A distinctive feature of the mentioned devices is their relatively narrow frequency band of operation, and high sensitivity.[3] The sensing of electromagnetic radiation at THz frequencies requires a rather nonconventional approach. For instance, in time-resolved coherent THz spectroscopy, the most popular technique involves the use of photoconductive antennas[4] gated by an ultrashort laser pulse delayed with respect to the exciting beam. The correlation between the excitation and the detection pulses allows one to monitor the evolution of the THz signal. Another method, free-space electro-optic sampling,[5] avoids the influence of the resonant nature of the dipole structure on the detection bandwidth and the spectral response, thus enabling coherent detection of THz transients within a very broadband (100 GHz–30 THz) range of frequencies.[6] On the other hand, both these optical-based methods require precise alignment of the setup and coherence between the optical and the THz radiation. As an alternative, one can use an interferometric technique,[7] but in this instant the detection system remains complicated, too, and, therefore, is not practical for direct applications in commercial sensors.

Thus, an electronic method of THz detection seems much more attractive as devices can be compact and compatible with other semiconductor elements—the property desired by electronic circuits designers. In general, detection can be realized in several different ways. The pyroelectrical sensing,[8] GaAs Schottky-barrier and metal-insulator-metal diodes in video detection and mixing[9] represent well-known and widely applied principles. Carrier heating by THz fields, which modify current flow, for example, through GaAs/AlGaAs coupled-quantum wells is used in biased p-i-n photodiodes.[10] Several new devices employ the transitions between either anti-crossing energy levels in GaAs/AlGaAs coupled-quantum-well photodiodes,[11] or between subbands having different electron mobilities in the so-called TACIT devices.[12] Finally, THz radiation can be recorded using GaAs multilayer p-p^+ junctions as active elements in homojunction interfacial workfunction thermal photoemission detectors,[13] or via THz-field induced modulation of Bloch oscillating miniband electrons in GaAs/AlAs superlattice based devices.[14]

In this article, we extend the existing concepts of electrical GHz–THz sensing: the idea of an asymmetrically shaped planar GaAs diode which contains a n-n^+ junction is introduced. The operation is based on nonuniform carrier heating effects which arise due to the shape and doping profile of the diode. The detector displays useful operational bandwidth ranging from 30 GHz up to 2.5 THz at room temperature. Additionally, the device can, in principal, be used to detect high radiation levels at frequencies reaching 30 THz.

The commercial products, e.g., broadband microwave-millimeter wave sensors and ground penetrating radar sys-

[a]Author to whom correspondence should be addressed; electronic mail: valusis@uj.pfi.lt

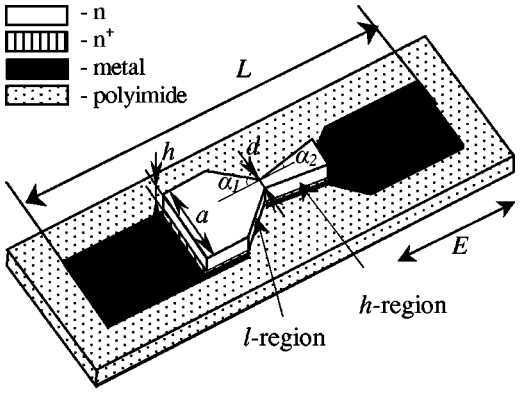

FIG. 1. Schematic view of the fabricated asymmetrically necked planar n-n^+-GaAs diode on 10-μm-thick polyimide film. Dimensions of the diode: $L=500$ μm, lengths of the ℓ region and h region are 100 μm each, width of the necked-part $d=12$ μm, thickness of the diode $h=3$ μm, width of the device $a=100$ μm, angles $\alpha_1=45°$; $\alpha_2=8°$. ℓ region is n doped close to 10^{15} cm^{-3}, h region is doped to $n^+=2\times10^{18}$ cm^{-3}. Thickness of n^+-GaAs and Ge–Au–Ni contact layers is 1 and about 0.5 μm, respectively. E direction indicates the orientation of the electric field of the incident electromagnetic radiation.

tems, require devices with a plateau over a wide frequency range, robustness and minimum maintenance electronics. The devices described here fulfill all these requirements: their sensitivity is nearly constant in the frequency range 30 GHz–0.7 THz at room temperature, they exhibit high robustness: there is no observable change in the device properties up to an illumination of 1 W microwave power in continuous wave regime and human static discharge brought about no failure in the diode operation. Since the external radiation induces a voltage signal over the ends of the device, no bias voltage is required for its operation. Furthermore, the choice of planar construction allows one to reach impedance matching in a simpler way and enable a minimization of design-limited effects, such as layer contact resistances due to small size of the electrical contacts (inherent for whisker-type diodes).

In this study, we give a report of systematic experimental study across the GHz–THz range at room temperature. A phenomenological model that explains diode operation in all frequency ranges is also presented. Ways to improve the sensitivity of the sensors are also discussed.

II. FABRICATION TECHNOLOGY AND MEASUREMENT TECHNIQUES

The asymmetrically necked devices (see Fig. 1) were manufactured on the base of a n-n^+-GaAs epitaxial structure using a photolithography process. Metal contacts for the diodes were produced by Ge–Ni–Au thermal evaporation, while metallic patterns were formed using a direct lift-off technique. The metal contacts were then annealed in an inert gas atmosphere. The asymmetrically formed semiconductor structures were covered with polyimide material by a spin-on technique and afterwards were cured at 250 °C for 1 h in order to obtain an elastic polyimide film of 10 μm thickness to serve as a mechanical support layer for the finished device. After thinning the semiconductor substrate to a desirable thickness by chemical etching, the semiconductor wafer was removed by wet etching from the ends of the metal contacts. In order to reduce the electrical resistance of the diode and to improve its impedance matching with the waveguides, the narrower part of the semiconductor structure (denoted in Fig. 1 as h region) was doped at 2×10^{18} cm^{-3} (n^+ region), keeping the carrier concentration in the n region (labeled as ℓ region in Fig. 1) close to 10^{15} cm^{-3}.

The resulting array of diodes, each with a length L of 500 μm, thickness h of 3–5 μm, width a of 100 μm and with the necked-part width d of about 10–18 μm, was then sliced into separate diodes. The devices were tested electrically by measuring the electrical resistances and $I-V$ characteristics. The latter served mainly for the estimation of the voltage sensitivity of the diode in dc fields according to a method described in Ref. 15: The voltage sensitivity S and the asymmetry of the $I-V$ characteristic of the device are related by $S=\Delta R/2U$, where ΔR is the difference in the resistance under forward and reverse bias U. Typical values of the sample resistance R were 3–5 kΩ, and the voltage sensitivity calculated from the $I-V$ characteristics was in the range $S=5-8$ V/W. In further experiments we selected eight samples with the following parameters: $R=3.5-4$ kΩ, necked-part width $d=12$ μm and $S\approx5$ V/W.

For GHz frequencies, i.e., 26-37.5 and 129-143 GHz, the measurements were performed with klystron-lamp generators which delivered pulsed signals of several microseconds duration at a 40 Hz repetition rate. In this band the diodes were placed in rectangular waveguides and oriented along their narrower walls. The induced signal was monitored by an oscilloscope.

In the THz band in the continuous wave (cw) regime, we employed a CO_2 pumped cw THz-laser emitting radiation at fixed frequencies of 0.693, 1.41, 1.63 and 2.52 THz. To guide the incident radiation into the freely mounted sample, a polyethylene lens was used. Coupling of the radiation with the detecting part of the sample was realized by shaping the diode as a bow-tie antenna. The signal was measured by a lock-in amplifier at a chopper frequency of 35-40 Hz.

In pulsed mode at 30 THz, the freely mounted sample was illuminated by a Q-switched CO_2 laser radiation at 10.6 μm wavelength. The pulse duration was 200 ns, while the repetition rate was 40 Hz. The signal was measured by an oscilloscope.

In all the experiments the electric field was oriented along the sample (E direction as indicated in the Fig. 1). All the measurements were performed at room temperature.

III. PRINCIPLE OF DEVICE OPERATION

The physics of the operation can be easily understood from Fig. 2, where a schematic view of the sample shape, the distribution of the electric field and the average electron energy are shown. We will consider physical processes in asymmetrically shaped, but otherwise *homogeneous* n-type semiconductor samples under an additional external voltage. It is evident from Fig. 2(b) that in the region x_1-x_2 the electric field is strongly nonuniform in comparison to that in the x_2-x_3 region where the gradient in the electric field is much lower. As a result, under forward bias (denoted as case 1 in

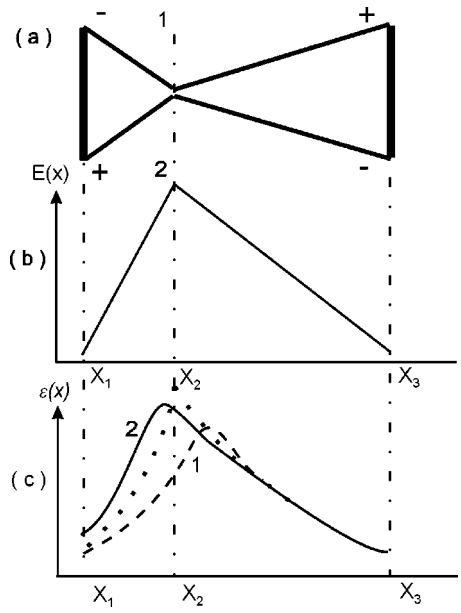

FIG. 2. Schematic view of the device shape (a), distribution of the electric field (b) and average electron energy (c) along the sample. Numbers 1 and 2 show the forward and the reverse polarity of the applied voltage, respectively. For comparison, the dotted line in part (c) depicts the average electron energy if the electric field is assumed to be uniform.

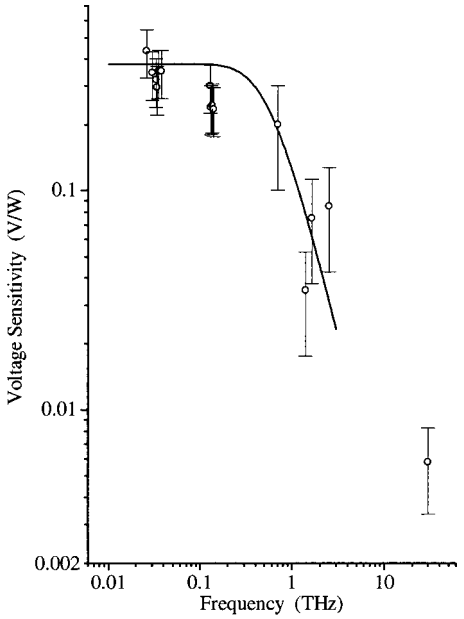

FIG. 3. Frequency dependence of the voltage sensitivity of the diode at room temperature. Solid curve calculations within the phenomenological approach assuming the absorption of 2.5% of the incident power. Points show the experimental data.

parts *a* and *c* of Fig. 2), the average electron energy $\varepsilon_1(x)$ at the distance x is smaller than the average steady state energy $\varepsilon(E)$ in a uniform electric field $E=E(x)$, as depicted in Fig. 2(c) by a dotted line. Thus, in the region $x_1 \leqslant x \leqslant x_2 + L_\varepsilon$, where L_ε is the product of the electron drift velocity and the energy relaxation time, the inequality $\varepsilon_1(x) < \varepsilon(E)$ is fulfilled. Usually, electron carrier mobility decreases with an increase of the average electron energy, therefore, the situation $\mu_1(x) > \mu(E)$ is realized. The quantities $\mu_1(x)$ and $\mu(E)$, similarly, designate electron mobility as a function of the coordinate in the constricted region and the respective mobility in a uniform electric field.

For the reverse bias, labeled as case 2 in parts *a* and *c* of Fig. 2, the average electron energy $\varepsilon_2(x)$ in the region x_1-x_2 is larger than $\varepsilon(E)$. Therefore, in the range, $x_1 \leqslant x \leqslant x_2 + L_\varepsilon$, the electron mobility in the forward current is larger than that in the reverse one, i.e., $\mu_1(x) > \mu_2(x)$. The electron mobility in strongly nonuniform electric fields depends both on the electric field and its gradient. As a result, the forward current I_f is larger than reverse one I_r at the same absolute value of the applied voltage. In other words, the asymmetrically necked structure fabricated from a homogeneous semiconductor displays the asymmetry in the I-V characteristics. This is one reason why high-frequency field is rectified and produces a dc voltage signal (or, so-called bigradient electromotive force) over the ends of the sample. This effect is used to detect electromagnetic radiation.

For detection within a wide frequency band and for higher sensitivity and operational speed, it is favorable to use GaAs-based structures, due to the high electron mobility in this material. Moreover, certain modifications, for example, additional doping of the necked part of the sample (shown as *h* region in Fig. 1) are desirable in order to reduce the resistance of the sample and to create an additional source of the voltage signal (due to conventional thermoelectromotive force of hot carriers in n-n^+ junction at high-frequency electric fields).

IV. EXPERIMENTAL RESULTS AND DISCUSSION

The frequency dependence of the device sensitivity is shown in Fig. 3. Several specific features can easily be distinguished. First, within the range from 30 up to 143 GHz the experimental voltage sensitivity is nearly independent of the frequency and is close to 0.3 V/W; second, in the THz range, the sensitivity decreases from 0.2 to 0.06 V/W; third, under infrared illumination at 30 THz, the sensitivity drops down to 6 mV/W. Before each of these points is discussed, we present a short description of the theoretical model which explains the experimental data.

To describe the frequency dependence of the device, according to Ref. 16, we applied the phenomenological approach based on equations of the current density, heat balance, heat flow density and Poisson's equation. Within the warm electron approximation, the voltage sensitivity S of the diode (defined as $S=U_d/P_i$, where U_d is the detected signal and P_i is the incident electromagnetic power) is

$$S = \frac{2\rho^n \mu_0 \tan\alpha_1}{3hd^2 \ln(1+a/d)} \frac{P}{P_i} N. \tag{1}$$

Here ρ^n labels the resistivity of the n region, μ_0 refers to the low-field electron mobility, P is the power absorbed by the diode, and N is the quantity, which determines the dependence of U_d on angular frequency ω of the electromagnetic radiation. Other symbols can be found in Fig. 1. (Note that due to the relatively highly doped h region of the diode there is no dependence on the angle α_2 in this expression.) If the

electron energy relaxation time τ_ε does not depend on the electron density in the semiconductor, (this is true for most weakly and moderately doped semiconductors at room temperature), the parameter N in Eq. (1) can be expressed as

$$N=\left[\frac{1+(\omega\tau_M^n)^2}{(\omega\tau_M^n)^2}\left\{\tau_\varepsilon\left[1+\frac{s^2}{1+(\omega\tau_\varepsilon)^2}\right]\ln[1+(\omega\tau_M^n)^2]+\tau_M^n\left[\frac{3}{2}-\frac{s(1-s)(\omega\tau_\varepsilon)^2}{1+(\omega\tau_\varepsilon)^2}\right]\left[\frac{1}{\omega\tau_M^n}\arctan(\omega\tau_M^n)-\frac{1}{1+(\omega\tau_M^n)^2}\right]\right\}+\frac{s(1-s)\tau_\varepsilon}{1+(\omega\tau_\varepsilon)^2}\right]\frac{1}{1+(\omega\tau)^2}, \quad (2)$$

where s is the exponent in the dependence of the electron momentum relaxation time τ on the electron energy ε and τ_M^n denotes the Maxwell relaxation time in the n region of the n-n^+ junction.

For the estimation of the frequency dependence of the voltage sensitivity S, we have used the following parameters of n-GaAs: the resistivity $\rho=0.8\ \Omega$ cm, $\tau_\varepsilon=450$ fs,[17] electron momentum relaxation time was 200 fs, $\tau_M^n=910$ fs, and $s=1$. Calculations have shown that the voltage sensitivity is nearly independent of the frequency up to 0.4 THz. At higher frequencies, the sensitivity decreases mainly due to the limit set by the momentum relaxation time (Fig. 3, solid line).

A. GHz frequencies

As is seen from Fig. 3, in the bands 26-37.5 GHz and 129-143 GHz, the experimental data on the sensitivity show good agreement with the theoretical estimations, if 2.5% of incident power is assumed to be absorbed by the diode.

The power absorbed can be evaluated from the voltage sensitivity obtained from the $I-V$ characteristics (the procedure is described in Sec. II) and comparing this value with the voltage sensitivity obtained from the microwave experiment directly. The voltage sensitivity of the diodes extracted from the $I-V$ curves was found to be about 5 V/W. Comparing this value with that obtained from the experiments we estimated that, depending on the sample, 2%-6% of the incident microwave power was absorbed under normal conditions. It is evident that the value of the theoretical estimate falls in the data interval given by the experiments.

A linear dependence of the voltage detected on the incident power at 30 GHz (Fig. 4, open circles) and at 129 GHz (Fig. 4, dark circles) demonstrates the suitability of the diodes in this range.

B. Cw mode at THz frequencies

At the frequencies of 0.693, 1.41, 1.63 and 2.52 THz, as Fig. 3 shows, the voltage sensitivity is also close to the values predicted by our phenomenological theory. Since in these experiments the sample was freely mounted, the power coupled by the device is needed to evaluate the sensitivity. It was estimated that a $(1\text{-}2)\times10^{-3}$ fraction of the incident power contributed to the voltage signal. The absorption by polyethylene lens was also taken into account.

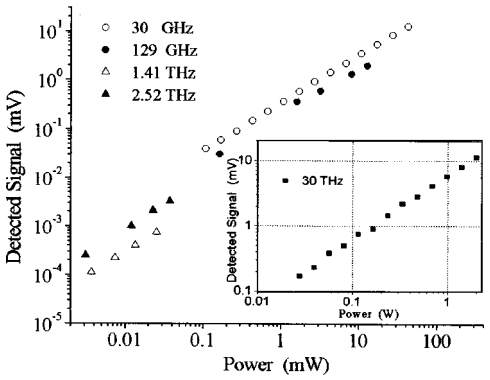

FIG. 4. Detector voltage as a function of power at room temperature at different frequencies: open circles −30 GHz, dark circles −129 GHz, open triangles −1.41 THz, dark triangles −2.52 THz. Inset: detector voltage as a function of power at room temperature under the pulsed illumination of 30 THz (10 μm wavelength).

The signal detected in the THz range, as in the GHz frequencies, linearly depends on the incident radiation power, as is shown in Fig. 4 by the open and dark triangles.

C. Pulsed high-intensity regime at 30 THz

As is known,[18] the intense CO_2-laser illumination increases the free carrier temperature in a semiconductor; this results in the formation of a photovoltage of hot carriers over the ends of the sample containing the n-n^+ junction. We found that a similar effect takes place in the asymmetrically necked n-n^+-GaAs samples: the infrared illumination induces a photoresponse, the polarity of which coincides with the hot-carrier and bigradient electromotive forces in a bulk semiconductor. Although the voltage-power dependence in this case was also found to be linear (see inset in Fig. 4), the value of the voltage sensitivity was found to be rather small: it was about 6 mV/W, if 1.3% of the incident power contributes to the signal. As is obvious from Fig. 4, this estimate is too far from that predicted by the phenomenological theory. We suppose that the discrepancy can be explained by other phenomena: at 30 THz, the reflectivity from the surface and the electron absorption cross section are both the functions of the photon energy. This was not taken into account in the phenomenological theory. Also, the size of the necked part of the sample, namely, 12 μm, is comparable to the wavelength of the incident laser light, hence, there additional antenna effects may appear. Therefore, the phenomenological approach is not sufficient at such high THz frequencies, and a more detailed quantum mechanical analysis is required to explain the signal magnitude.

V. COMPARISON WITH OTHER DEVICES AND WAYS TO INCREASE THE SENSITIVITY

To define the niche of our sensor in the family of available devices, we compare its salient features with the properties of other sensors operating in a similar frequency range at room temperature. In terms of the sensitivity, in the THz range, the asymmetrically shaped n-n^+-GaAs planar diodes are comparable with the GaAs/AlAs superlattice based sensors[14] and are better than the detectors containing the

field-effect transistor with two-dimensional electrons.[19] More specifically, the sensitivity of these devices at 2.5 THz is 10 mV/W, while our sensor exhibits the value of about 60-80 mW/W at the same frequency. Obviously, our device cannot compete with Schottky diodes. For example, those based on the Pt/n-GaAs junction[20] at 1 THz display a sensitivity value of 650 V/W. In our case, even if the size of the neck is reduced down to 300 nm, the sensitivity could be increased only up to the value of 18 V/W at 1 THz. On the other hand, this is close to the sensitivity of an antenna coupled Bi microbolometer operating on Si/SiO_2, which is about 25 V/W in the range of 1.62-4.25 THz.[21] As for other key features, for example, the resistance to overloading, our device can withstand 1 W of maximum applied power without any negative outcome. For comparison, one can note that this parameter for Pt/n-GaAs Schottky diode is about 1 mW.[20] Moreover, our sensor can work in a homodyne detection scheme and has a very broad frequency band of operation.

It is evident, however, that our proposed device suffers from rather low sensitivity. One of the possible ways to improve the sensitivity stems from Eq. (1) which shows that it is preferable either to use the material with a very high carrier mobility or to make the necked part narrower. The latter way seems to be more effective due to its stronger functional dependence on the neck width. We have calculated the voltage sensitivity at 0.15 THz for the asymmetrically necked sample of resistance 3.9 kΩ and 2.5% absorption of the incident power. To keep the absorption constant we assumed that the sample resistance did not change with geometry of the sample, since the decrease of the necked part may be compensated by a corresponding increase in the thickness of the sample. Estimates have shown that, for instance, at a width of the neck $d=300$ nm, one can reach a sensitivity higher than 50 V/W, i.e., more than two orders of magnitude higher than the experimental value obtained to date.

VI. CONCLUSIONS

In summary, a wide frequency band, from 30 GHz to 2.5 THz, detector based on an asymmetrically necked GaAs planar structure containing n-n^+ junction was proposed and implemented. The voltage signal over the detector is related to nonuniform heating of the free electrons caused by the external electromagnetic radiation. The voltage sensitivity of the detector from 30 GHz up to 0.7 THz is almost independent of the frequency and is about 0.3 V/W. At higher frequencies, it is limited by the electron momentum relaxation time and drops down to 80 mV/W at 2.5 THz. The presented investigations demonstrate that the bigradient and thermoelectric effects of the hot carriers can be successfully employed in wideband detection at room temperature. The design is not sufficiently optimal and improvements are possible to increase the voltage sensitivity.

ACKNOWLEDGMENTS

The authors highly appreciate kind and professional help in THz experiments from Bernd Wolf, Steffen Schmidt and Holger Schwenk. Also, the authors are greatly indebted to Vitaly Ksenevich, Robert Sachs, Gregor Segschneider and Mark D. Thomson for interesting and valuable discussions. Special thanks to Herbert Hassenflug for the help in the improvements of the experimental setup and Adolfas Dargys for critical reading of the manuscript. G. V. acknowledges Alexander von Humboldt Stiftung for financial support. From the Lithuanian side the work was supported, in part, by the Program ''Jutikliai.''

[1] M. Dagys, Ž. Kancleris, R. Simniškis, E. Schamiloglu, and F. J. Agee, IEEE Antennas Propag. Mag. **43**, 64 (2001).
[2] Fundamentals of rf and Microwave Power Measurements, Hewlett-Packard Application Note No. 64-1A, (1996).
[3] B. F. Levine, J. Appl. Phys. **74**, R1 (1997).
[4] D. Grischkowsky, S. Kleiding, M. van Exter, and Ch. Fattinger, J. Opt. Soc. Am. B **7**, 2006 (1990).
[5] Q. Wu and X. C. Zhang, Appl. Phys. Lett. **67**, 3523 (1995).
[6] P. Y. Han and X. C. Zhang, Appl. Phys. Lett. **73**, 3049 (1998).
[7] B. I. Green, J. F. Federici, D. R. Dykaar, R. R. Jones, and P. H. Bucksbaum, Appl. Phys. Lett. **59**, 893 (1991).
[8] E. Budiarto, J. Margolies, S. Jeong, J. Son, and J. Bokor, IEEE J. Quantum Electron. **32**, 1389 (1996).
[9] H.-W. Hübers, G. W. Schwaab, and H. P. Röser, J. Appl. Phys. **75**, 4243 (1994).
[10] R. J. Stone, J. G. Michels, S. L. Wong, C. T. Foxon, R. J. Nicholas, and A. M. Fox, Appl. Phys. Lett. **69**, 3569 (1996).
[11] A. M. Tomlinson, C. C. Chang, R. J. Stone, R. J. Nicholas, A. M. Fox, M. A. Pate, and C. T. Foxon, Appl. Phys. Lett. **76**, 1579 (2000).
[12] C. L. Cates, G. Briceño, M. S. Sherwin, K. D. Maranowski, K. Campman, and A. C. Gossard, Physica E (Amsterdam) **2**, 463 (1998).
[13] A. G. U. Perera, H. X. Yuan, S. K. Gamage, W. Z. Shen, M. H. Francombe, H. C. Liu, M. Buchanan, and W. J. Schaff, J. Appl. Phys. **81**, 3316 (1997).
[14] E. Schomburg, F. Klappenberger, M. Krätschmer, A. A. Ignatov, K. F. Renk, and W. Wegscheider, *Proc. 8th International Conference on Terahertz Electronics*, edited by Chih-I Lin, M. Rodriguez-Girones, and V. Ichizli (VDE, Darmstadt 2000), p. 91.
[15] S. Ašmontas and A. Sužiedelis, Int. J. Infrared Millim. Waves **15**, 525 (1994).
[16] S. Ašmontas and A. Sužiedelis, Int. J. Infrared Millim. Waves **1**, 5 (1997).
[17] V. Dienys, S. Dedulevič, Ž. Kancleris, Z. Martūnas, and A. Šetkus, Lith. J. Phys. **29**, 46 (1989).
[18] S. Ašmontas, J. Gradauskas, D. Seliuta, A. Šilenas, and E. Širmulis, *Proc. GaAs and Related III–V Compunds Symp.*, edited by C. Rumelhard, Paris (CNAM, Paris, 1996), Vol. 3B1.
[19] J.-Q. Lü, M. S. Shur, J. L. Hesler, L. Sun, and R. Weikle, IEEE Electron Device Lett. **19**, 373 (1998).
[20] J.-J. Chang, T. Nozokido, Ch. M. Mann, T. Suzuki, and K. Mizuno, RIKEN Rev. **11**, 9 (1995).
[21] F. Ghianni, T. O. Klassen and W. Th. Wenckebach, *Proc. of the Symposium on IEEE/LEOS Benelux Chapter* (Mons, Belgium, 1999), p. 99.